International Journal of Bridge Engineering (IJBE), Vol. 2, No. 1, (2014), pp. 17-42

ANALYSIS OF INCREMENTALLY LAUNCHED BRIDGES: A PARAMETRIC MATRIX BASED STUDY

Arman Shojaei [1], Hossein Tajmir Riahi [2] and Siavash Haji Akbari Fini[3]

[1] Isfahan University of Technology, Dept. of Civil Engineering, Iran
[2] Univeristy of Isfahan , Dept. of Civil Engineering, Faculty of Engineering, Iran
[3] University of British Columbia, Dept. of Civil Engineering, Canada

a.shojaei@cv.iut.ac.ir, tajmir@eng.ui.ac.ir, s.hajiakbarifini@alumni.ubc.ca

ABSTRACT: Incremental bridge launching is a widespread bridge construction method which may offer many advantages over conventional ones. In this technique, during phases of construction, internal forces of deck which may be more critical in comparison with those applied in service time, vary frequently. Therefore, an appropriate method shall be applied to reduce these forces and avoid eliminating the advantages of the method due to overdesigned structural members. For this purpose, using a nose-deck system is known as the standard method. In addition, mechanical and geometric characteristics of the launching nose are determinative based on launching stresses. Therefore, it is essential to carry out an optimal design procedure for the nose. In this paper, a new model based on matrix structural analysis is presented for the study of static behavior of bridge during launching stages. Also a simple method is introduced to scale all quantities in the procedure. Likewise, a simple model as a "semi-infinite beam" is introduced, which is useful for studying nose-deck interaction. Consequently, optimum design of the launching nose has been investigated through this model via a simple mathematical approach. It is shown that the accuracy of this model may not be satisfactory for initial stages of launching (or bridges with few numbers of spans). Therefore, some solutions are suggested to preserve the efficiency of the optimized nose for all stages of launching, in the view of optimum static performance of the bridge in service time.

KEYWORDS: Bridges; Incremental bridge launching; Semi-infinite beam; Nose–deck system; Optimization; Matrix Structural Analysis.

1 INTRODUCTION

In incremental bridge launching, bridge piers are constructed first; then deck parts are pushed forward above them to be installed at their final positions (Fig. 1). All the related activities such as constructing, concrete molding, curing and

pushing deck segments are executed on the construction platforms, close to bridge abutments [2], [3]. Applying this method will lead to advantages such as high speed work by eliminating castings, reducing manpower and costs, high qualified inspections by supervisors, no need to block the roads under the bridge during work, and reducing the hazardous activities to the environment. Furthermore, taking deck segments length over a half-length of the bridge span reduces the structural weak points in junctions, which is highly important in seismic design. This will lead incremental launching to be more competitive [4], [5], [6].

Figure 1. Incremental bridge launching [1]

To design an incrementally lunched bridge two forces should be taken into account i.e. temporary and permanent forces. The former refers to ones which are created during construction (dead loads, thermal gradients and bearing settlements) and the latter refers to service life. In comparison to service life, temporary forces can be different and more critical. Therefore a suitable method should be applied to reduce these forces and prevent the elimination of advantages of the method due to overdesigned structural elements. For this purpose, various methods have already been developed by engineers. Among them, nose-deck system is regarded as a standard method for its efficiency and economic features. In nose-deck system, a light nose girder connected in front of the deck is applied to reduce the cantilever moment at its end [2]. Nose specifications play a very important role in nose-deck interaction. Thereupon, choosing proper parameters will decrease the internal forces in the girder and will considerably save material and costs. It should be noted that some practical methods such as temporary prestressing and applying temporary piers can avoid

overdesigning elements but usually nose deck system is preferred due to some problems of the mentioned methods [5]. As an example, since during bridge lunching all segments experience cyclic change of bending moments and shear forces, parabolic tendons scheme is not useful. Rosignoli indicated suitable prestressing schemes for incrementally launched bridges in [7], and Sasmal et al studied the effect of these prestressing forces on variation of moment during launching [8].

Two main types of analysis for incremental bridge launching can be found in the literature. The first type deals with the nose-deck interaction and optimization of the nose parameters. In this regard, a simple model of the nose-deck system is provided. Marchetti applied the elastic load analysis, and presented a simplified model of launching bridge [9]. Rosignoli studied nose-deck interaction of launched bridge and investigated the optimum nose specifications via a trial and error approach [5]. More recently, Fontan et al have dealt with the optimum nose specification based on Marchetti model with mathematical optimization approaches [10].

The second type of analysis corresponds to the methods and algorithms for the analysis of the bridge during launching. Pushing forward the deck system above the piers leads the designer to the analysis of the structure in different schemes and pier arrangements. It should be pointed out that the best method is the fastest and the most convenient one for computer programming; moreover, it should outgrowth the most information in the least possible time.

Rosignoli introduced an effective algorithm for the simulation of incremental bridge launching via RTM (Reduced Transfer Matrix) method [11]. Sasmal et al presented TTM (Transient Transfer Matrix) method for the analysis of a bridge [12]. Afterwards, Sasmal et al extended this method for the prestressed concrete bridges [6]. Arici et al and Granta et al improvised TTM method for the analysis of curved box concrete bridges in which curved bridges with complex geometries can be considered [13], [14].

This paper presents a method based on structural matrix analysis to model incremental launching for the both types mentioned above. It is shown that not only does this method share some advantages with RTM and TTM, but also it can be methodical and convenient for computer programming, from designers points of view. A simple method is applied to scale all parameters in the model based on deck main parameters. In addition, some factors such as shear deformation on the beam and temperature gradient effects are studied. Also, a simplified model is introduced named as “Semi Infinite Beam” model. This model is useful for studying nose-deck interaction, and finding optimum ranges for nose parameters. However, it is demonstrated that the simplified model has

some limitations based on this fact that it cannot be accurate enough for initial stages of launching and as well as bridges with a few number of spans. As a repercussion, some solutions are presented to improve it during launching of initial spans of the bridges. It is shown, the condition for initial stages of launching may be more critical than farther mid spans; for this reason, optimum performance of nose, obtained based on conventional semi-infinite beam model, may deteriorate. In this regards, some remedies are suggested to address such a restriction.

2 ASSUMPTIONS AND DEFINITIONS

In this study, some assumptions are adopted to develop matrix structural analysis as follows.

2.1 Piers arrangement scheme

Various distributions for piers can be considered in the model. However, it is more logical to locate the fixed piers on the basis of optimum performance of bridges during their service times. Forces during the construction time can be reduced using other practices such as providing a light nose girder, prestressing or applying temporary piers. In this paper, the bridge structure is comprised of identical mid spans and shorter end ones (See Section. 6). It is worthwhile to mention, majority of bridges with continuous structural systems has been erected with respect to this pattern due to its structural and architectural benefits. However, this model is not restricted to such an assumption, as one can consider any scheme for piers arrangement.

2.2 Definition of stage, station and phase

The nose tip forwards through all spans during launching. The number of launching spans is defined as the launching stage; furthermore, station is defined as the number of piers behind the launching stage. Two different phases can be considered for each stage. Phase one introduces the position that nose tip has not reached the next pier. In addition, the nose-deck system has a cantilever behavior at its end. This phase continues until the nose tip meets the next pier. Phase two takes the position after that and continues until nose girder meets the next pier. Definitions of stage, station and phases are illustrated in Fig. 2.

2.3 Defining nose parameters

Although most noses are constructed with non-prismatic sections, the nose girder is assumed to be prismatic. Using mean values of the non-prismatic nose specifications for the equivalent prismatic one will cause very small errors (less than 2%) [15], [16]. Therefore, this simplification is accurate enough. Flexural

stiffness, dead load, length and height of nose are denoted by $E_n I_n$, q_n, L_n and H_n, respectively.

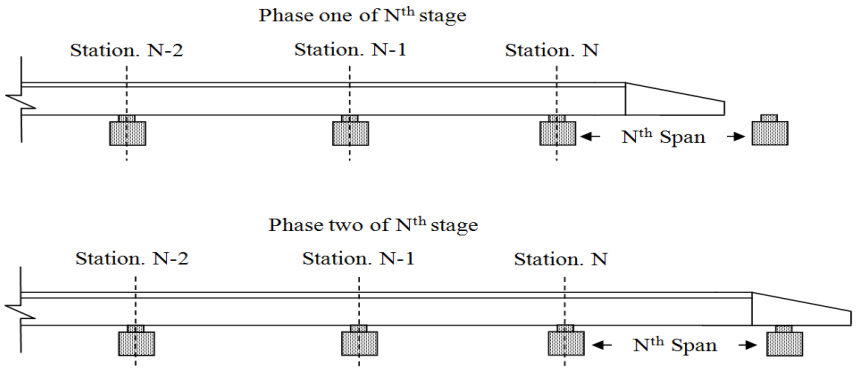

Figure 2. Definition of station, stage and phases.

2.4 Scaling on the basis of deck parameters

Three main deck parameters including flexural stiffness ($E_D I_D$), dead load (q_D) and mid spans length (L_D) have been taken as the measuring scales. Therefore, other quantities in the problem can be calculated with respect to these values. Consequently, L_n, q_n, $E_n I_n$ and H_n in the scaled format are presented by four dimensionless parameters, β_L (ratio of nose length to mid span one, L_D/L_n), β_q (ratio of nose load to deck one, q_D/q_n), β_{EI} (ratio of nose flexural stiffness to deck one, EI_D/EI_n) and β_{HN} (ratio of nose section height to mid span one, H_n/L_D). This approach can represent unknown variables as a function of deck parameters. To elucidate, the internal moment deck sections are obtained with the coefficient of $q_D L_D^2$. Length of end spans and deck height in the scaled format are denoted by β_1 (ratio of length of first span to mid span one) and β_{HD} (H_D/L_D), respectively. This simple technique provides the analysis procedure to be completely independent of some important fundamental designing factors; in other words, the whole procedure is summarized with respect to the relation between deck and nose geometrical and mechanical parameters. Therefore, the foregoing procedure can be used easily for parametric studies of nose-deck interaction. It should be remarked here such

a treatment can also be applied to other solution methods such as RTM and TTM.

2.5 Deck specifications

It is assumed that the bridge is straight and without horizontal curvilinear. In most cases, especially for highway bridges, use of box girders is common. Since box girders have high torsional rigidity, the torsional moment effect can be neglected for bridges during launching. Therefore, the straight beam theory will become acceptable [11]. Additionally, mechanical specifications are assumed to be identical along the lengths of the deck.

Since all deck sections periodically undergoes negative and positive moments during launching; it is rational to use a central prestressing scheme. This central prestressing will not influence internal bending moments of the deck. Therefore, it can be determined regardless of this prestressing. In practice, after launching is processed, a proper parabolic prestressing scheme can be substitute for central one.

Prestressed composite bridges may experience significant deflections due to shear slips arise out of shear studs located between steel girders and concrete slabs [2], [17], [18]. In this study, the effects of shear slip are not taken into account; however, shear deformations on the beam (Timoshenko beam) have been investigated.

2.6 Construction platform modeling

On average one or two deck segments are kept on construction platform during launching. Although, the platform is located on the prefabrication yard, when nose reaches piers, axial stiffness of platform supports can be neglected versus very high axial stiffness of bridge piers and thus the platform supports can be ignored. Thereupon, concentrating shear force and moment on the first station can be substituted for the tail of the bridge (sections between platform and first pier). Average length of segments on the platform, L_0, is denoted by scaled parameter β_0 (L_0/L_D).

3 FORMULATION

Usual beam elements with two end nodes have two degrees of freedom in each node. In these elements, axial degree of freedom is not considered. It should be noted that axial stiffness of deck is high and its axial force is relatively small; therefore, axial displacements are negligible and usual beam elements are sufficient to model the continuous deck of the bridge.

In this section, bold letters refer to matrix variables. For a beam element shown in Fig. 3, nodal forces vector, $\mathbf{f}$, and displacements vector, $\mathbf{d}$, are defined as follow:

$$\mathbf{f} = \langle \mathbf{f}_i \quad \mathbf{f}_j \rangle^T, \quad \mathbf{f}_i = \langle f_1 \quad f_2 \rangle^T, \quad \mathbf{f}_j = \langle f_3 \quad f_4 \rangle^T \tag{1}$$

$$\mathbf{d} = \langle \mathbf{d}_i \quad \mathbf{d}_j \rangle^T, \quad \mathbf{d}_i = \langle d_1 \quad d_2 \rangle^T, \quad \mathbf{d}_j = \langle d_3 \quad d_4 \rangle^T \tag{2}$$

Using stiffness method, matrix analysis formulation can be written as:

$$\mathbf{f} - \mathbf{f}_f = \mathbf{k}.\mathbf{d}, \quad \mathbf{f}_f = \mathbf{f}_q + \mathbf{f}_t \tag{3}$$

where $\mathbf{k}$ is the global stiffness matrix of the element, $\mathbf{f}_f$ is summation of $\mathbf{f}_q$ (equivalent element nodal forces vector due to external distributed loads) and $\mathbf{f}_t$ (equivalent element nodal forces vector due to thermal loads).

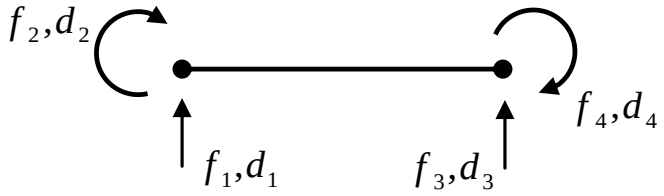

Figure 3. Beam Element

Global stiffness matrix of elements with constant section properties is as follows [19]:

$$\mathbf{k} = \mathbf{T}^T \mathbf{k}' \mathbf{T} = \begin{bmatrix} \mathbf{s}_{ii} & \mathbf{s}_{ij} \\ \mathbf{s}_{ji} & \mathbf{s}_{jj} \end{bmatrix} \tag{4}$$

where:

$$\mathbf{S}_{ii} = \mu\begin{bmatrix} \frac{12}{L} & 6 \\ 6 & \frac{4\left(L^2 + 3EI\,\frac{\bar{\tau}}{GA}\right)}{L} \end{bmatrix}, \quad \mathbf{S}_{ij} = \mu\begin{bmatrix} -\frac{12}{L} & 6 \\ -6 & \frac{2\left(L^2 - 6EI\,\frac{\bar{\tau}}{GA}\right)}{L} \end{bmatrix},$$
$$\mathbf{S}_{ji} = \mu\begin{bmatrix} -\frac{12}{L} & -6 \\ 6 & \frac{2\left(L^2 - 6EI\,\frac{\bar{\tau}}{GA}\right)}{L} \end{bmatrix}, \quad \mathbf{S}_{jj} = \mu\begin{bmatrix} \frac{12}{L} & -6 \\ -6 & \frac{4\left(L^2 + 3EI\,\frac{\bar{\tau}}{GA}\right)}{L} \end{bmatrix} \tag{5}$$

$$\mu = \frac{EI}{L^2 + 12EI\,\frac{\tau}{GA}} \tag{6}$$

E and G are modulus of elasticity and shear of the material, I and A are moment of inertia and area of the section, L is the length of the element and $\bar{\tau}$ is the shear constant (ratio of maximum shear stress to average one at the section). $\mathbf{k}'$ stands for the local stiffness matrix of the element defined as follows:

$$\mathbf{k}' = EI\begin{bmatrix} \frac{1}{L} + \frac{3AGL}{AGL^2 + 12EI\,\bar{\tau}} & -\frac{1}{L} + \frac{3AGL}{AGL^2 + 12EI\,\bar{\tau}} \\ -\frac{1}{L} + \frac{3AGL}{AGL^2 + 12EI\,\bar{\tau}} & \frac{1}{L} + \frac{3AGL}{AGL^2 + 12EI\,\bar{\tau}} \end{bmatrix} \tag{7}$$

, and $\mathbf{T}$ is the transformation matrix defined as:

$$\mathbf{T} = \begin{bmatrix} 1/L & 1 & -1/L & 0 \\ 1/L & 0 & -1/L & 1 \end{bmatrix} \tag{8}$$

Considering a uniform distributed load on the element and linear thermal gradient, $\mathbf{f}_q$ and $\mathbf{f}_t$ vectors can be stated as [19]:

$$\mathbf{f}_q = \left\langle \frac{qL}{2} \quad \frac{qL^2}{12} \quad \frac{qL}{2} \quad -\frac{qL^2}{12} \right\rangle^T \tag{9}$$

$$\mathbf{f}_t = \frac{EI.\alpha_T.\Delta T}{H}\langle 0 \quad -1 \quad 0 \quad -1\rangle^T \tag{10}$$

where q, ΔT, H and α_T are uniform distributed load on the element per unit length, difference between the temperature at top and bottom of the section, height of the section and thermal expansion coefficient, respectively. It should be noted all terms can be scaled with respect to the deck parameters as is discussed.

Shear stiffness is only considered for the concrete deck section and is neglected in the nose girder. $\bar{\tau}/GA$ term which shows the effects of shear deformation in stiffness matrix, can be written as:

$$\begin{aligned} &\frac{\bar{\tau}}{GA} = {L_D}^2 \Big/ E_D I_D \; \beta_s \beta_r^2 \equiv \beta_s \beta_r^2, \quad E_D I_D = 1, \quad L_D = 1, \\ &\beta_r = \frac{r_{gyr}}{L_D}, \quad \beta_s = 2\bar{\tau}(1+\upsilon) \end{aligned} \tag{11}$$

r_{gyr} and υ are radius of gyration of the deck section and Poisson ratio of the deck material.

As an example, the stiffness matrix of first element (first bridge span), in scaled format considering $L = \beta_1$ and $EI = \beta_{EI}$, can be written as follows:

$$\mathbf{s}^{el\,1} = T^T k' T =$$

$$\begin{bmatrix} \frac{12\beta_{EI}}{\beta_1^3 + 12\beta_1\beta_{EI}\beta_r^2\beta_s} & \frac{6\beta_{EI}}{\beta_1^2 + 12\beta_1\beta_{EI}\beta_r^2\beta_s} & -\frac{12\beta_{EI}}{\beta_1^3 + 12\beta_1\beta_{EI}\beta_r^2\beta_s} & \frac{6\beta_{EI}}{\beta_1^2 + 12\beta_1\beta_{EI}\beta_r^2\beta_s} \\ & \frac{\beta_{EI}}{\beta_1} + \frac{3\beta_1\beta_{EI}}{\beta_1^2 + 12\beta_1\beta_{EI}\beta_r^2\beta_s} & -\frac{6\beta_{EI}}{\beta_1^2 + 12\beta_1\beta_{EI}\beta_r^2\beta_s} & -\frac{\beta_{EI}}{\beta_1} + \frac{3\beta_1\beta_{EI}}{\beta_1^2 + 12\beta_1\beta_{EI}\beta_r^2\beta_s} \\ & & \frac{12\beta_{EI}}{\beta_1^3 + 12\beta_1\beta_{EI}\beta_r^2\beta_s} & -\frac{6\beta_{EI}}{\beta_1^2 + \beta_1\beta_{EI}\beta_r^2\beta_s} \\ \text{SYM} & & & \frac{\beta_{EI}}{\beta_1} + \frac{3\beta_1\beta_{EI}}{\beta_1^2 + 12\beta_1\beta_{EI}\beta_r^2\beta_s} \end{bmatrix} \tag{12}$$

Superscript *el* denotes the element number. As can be seen, the stiffness matrix arrays are obtained based on the deck parameters only. The final global system of equation governing the problem can be written as:

$$\mathbf{F} - \mathbf{F}_f = \mathbf{K}.\mathbf{D} \tag{13}$$

where $\mathbf{K}$ is the global stiffness matrix, $\mathbf{F}$ is the global nodal forces vector, $\mathbf{F}_f$ is the global equivalent nodal forces vector and $\mathbf{D}$ is the global nodal

displacement vector. Support settlement of a generic pier, δ_i , can be imposed directly by replacing their scaled value, δ_i / L_D in the appropriate row of $\mathbf{D}$.

Numbering of elements is started from the first span of the bridge and continues to the last one; then $\mathbf{K}$ and $\mathbf{F}_f$ are assembled, from the predefined connectivity matrix of elements, as follows:

$$\begin{cases} \mathbf{K}(2a-1 \text{ to } 2a, 2a-1 \text{ to } 2a) = \mathbf{s}_{jj}^{el\ a-1} + \mathbf{s}_{ii}^{el\ a} \\ \mathbf{K}(2a-3 \text{ to } 2a-2, 2a-1 \text{ to } 2a) = \mathbf{s}_{ij}^{el\ a-1} \\ \mathbf{K}(2a-1 \text{ to } 2a, 2a-3 \text{ to } 2a-2) = \mathbf{s}_{ji}^{el\ a-1} \\ \mathbf{K}(otherwise) = 0 \end{cases} \quad , \quad \text{For } a = 1, 2, \ldots, \text{ number of elements} \tag{14}$$

$$\mathbf{F}_f\,(2a-1 \text{ to } 2a) = \mathbf{f}_{f\ j}^{el\ a-1} + \mathbf{f}_{f\ i}^{el\ a} \tag{15}$$

Remark I: Using the scaling technique and matrix structural analysis contributes the current study to be flexible and free of any restriction to the pattern of load distribution. The developed formulations of this study can be extended to analysis prestressed and horizontal curved bridges; it suffices to consider some modifications in element stiffness matrix. However, it is beyond the scope of this paper. ■

On the basis of equation (14), global stiffness matrix is obtained banded and calculation time of solving equation (13) is reduced significantly due to narrow band width of $\mathbf{K}$. This matter offers a lot of advantages for sparse array programming and shortening the computational time. A banded stiffness matrix (which is the result of the appropriate element numbering) compensates its higher dimensions in comparison to lower dimension matrices used in RTM and TTM methods. The RTM and TTM methods use fast and repetitive algorithms to satisfy boundary conditions of each element for each step of computation. Owing to these facts, these methods have benefits to limit the possible mistakes during analysis procedure [14]. In the present method, boundary conditions are directly imposed and the procedure is only summarized in building the global stiffness matrix and nodal forces vectors which eliminates such possible mistakes completely. As a result, the current study shares it's advantageous with fast repetitive algorithmic methods. Therefore, it is suitable for systematic computer analysis. Moreover, since most of the popular software packages perform based on structural matrix analysis platforms, engineers are more familiar with the current method procedure.

4 NOSE-DECK INTERACTION

4.1 Conventional semi-infinite beam model

Fig. 4 shows the envelope of the fifteenth station moment for different values of relative flexural stiffness (β_{EI}) with relative length (β_L) and relative load (β_q) as 0.8 and 0.1, respectively. This station is selected to ensure that it behaves as a station with infinite spans behind it. Nose end distance from the station under studies is denoted by α (Launching parameter) obtained with respect to mid span length. In phase one of launching (zone I), envelop of the moment is independent of nose flexural stiffness. Therefore, curves completely overlap with each other. On the contrary, in phase two (zone II) moment is dependent on β_{EI} drastically. It is noticeable as the launching proceeds and the nose tip gets a position about 3 spans farther than this station, moment is decreased to -1/12 (i.e. the scaled format of $qL^2/12$), and it reaches a plateau at this level. It is worth noting that when phase two is proceeding, the envelope of previous station moment (station 14th) is regarded as the start of zone III. Moreover, the moment of two former stations are stabilized at -1/12.

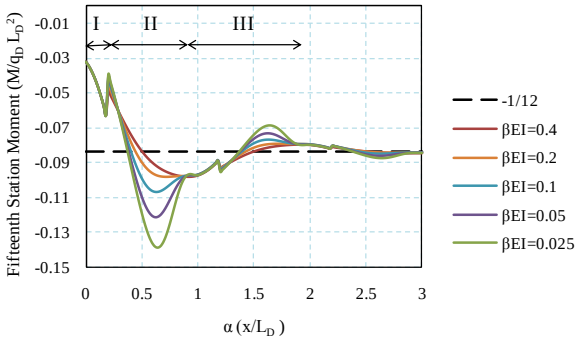

Figure 4. Envelope of the fifteenth station moment for $\beta_L = 0.8$, $\beta_q = 0.1$ and different values of β_{EI} .

Fig. 5 illustrates the envelope of the fifteenth station rotation. It should be noted that the entire story is similar to envelope of its moment. Moreover, as it is shown the rotation of the second former station approximately remains unchanged at zero. It can be concluded that two boundary conditions are arisen up for this station, and it leads to consider a simple semi-infinite continuous beam rather than the analysis of the whole structure (See Fig. 6a, b). It is remarkable that the developed simplified model has a lot of advantageous to be applied for investigation of nose ideal parameters. Majority of researchers

standardize this model as a prototype for optimization of nose specifications, as in [5], [10].

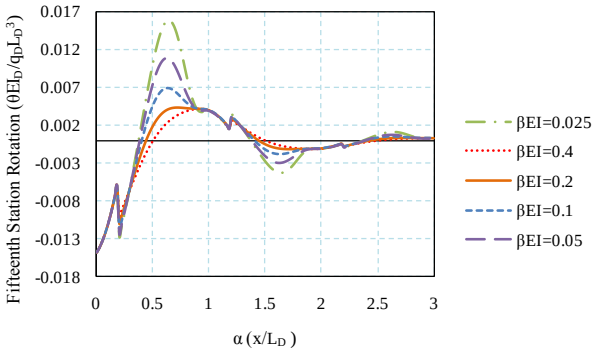

Figure 5. Envelope of the fifteenth station rotation for $\beta_L = 0.8$, $\beta_q = 0.1$ and different values of β_{EI}.

4.2 A simple mathematical approach to optimum design of nose parameters

The simple developed structure in the previous section can be analyzed through different structural analysis techniques such as theory of virtual work or slope-deflection method. However, for the sake of brevity, just the final results, in the scaled format, are presented.

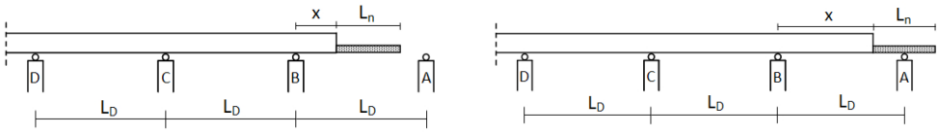

Figure 6. Semi-infinite beam model; a) Phase 1, b) Phase 2

In phase one of launching progression, $0 \le \alpha \le 1 - \beta_L$, station B undergoes a moment as:

$$M_{B,1} = -\frac{\alpha^2}{2} - \beta_q \beta_L \left(\alpha + \frac{1}{2}\beta_L\right) \tag{16}$$

where the second subscript denotes the number of launching phase. The moment of station C (back support) is obtained as follows:

$$M_{C,1} = \frac{1}{12}(-3+\sqrt{3}) + (-2+\sqrt{3})M_{B,1} \tag{17}$$

where, for station B the following reaction can be obtained:

$$R_{B,1} = M_{C,1} + \frac{(1+\alpha)^2}{2} + \beta_q \beta_L (1+\alpha+\frac{1}{2}\beta_L) \tag{18}$$

Once the nose tip meets station A, the redistribution of elastic deflection causes a positive moment that reduces station B moment. In this situation, the second stage of launching $1-\beta_L \le \alpha \le 1$, begins (See Fig. 6b). In this phase moment of station B is defined as follows:

$$M_{B,2} = \frac{(-\frac{1}{24\sqrt{3}} - C_3) + \frac{1}{2}\beta_q C_2 (\beta_L + \alpha - 1)^2}{\frac{1}{2\sqrt{3}} + C_1} \tag{19}$$

where:

$$C_1 = \frac{1}{3}\left[1 + (\frac{1}{\beta_{EI}} - 1)(1-\alpha)^3\right] \tag{20}$$

$$C_2 = \alpha^2(\frac{1}{2} - \frac{\alpha}{3}) + \frac{1}{\beta_{EI}}(\frac{1}{6} - \frac{\alpha^2}{2} + \frac{\alpha^3}{3}) \tag{21}$$

$$C_3 = \frac{1}{2}\left\{\left[\alpha(2-\alpha) + \beta_q(1-\alpha)^2\right]\left(\frac{\alpha^2}{2} - \frac{\alpha^3}{3}\right) - (\frac{\alpha^3}{3} - \frac{\alpha^4}{4})\right\} + \frac{1}{24\beta_{EI}}\left[4\alpha^2(1-\alpha)^3 + \beta_q(4\alpha^5 - 15\alpha^4 + 20\alpha^3 - 10\alpha^2 + 1\right] \tag{22}$$

Consequently, $R_{A,2}$ and $M_{C,2}$ can be obtained as follow:

$$R_{A,2} = M_{B,1} - M_{B,2} \tag{23}$$

$$M_{C,2} = \frac{5}{48} - M_{B,2} \tag{24}$$

Furthermore, using the equilibrium conditions in phase two of launching, the values of maximum positive bending moments in AB and BC spans (See Fig. 6b) can be determined as:

$$M_{AB}^{\max} = R_{A,2}(1+\alpha-\beta_q\beta_L)+\frac{1}{2}R_{A,2}{}^2+\frac{1}{2}\beta_q\beta_L{}^2(\beta_q-1) \quad (25)$$

$$M_{BC}^{\max} = \frac{1}{2}(M_{C,2}-M_{B,2}+\frac{1}{2})^2+M_{B,2} \quad (26)$$

It should be pointed out that the absolute maximum values for positive moments of AB and BC spans depend on launching parameter (α), and they do not occur at the same launching position. Absolute maximum positive moments in AB and BC spans are obtained as follows:

$$(M_{AB}^{\max})^{\max} = M_{AB}^{\max}\Big|_{\alpha=1-\beta_q\beta_L} \quad (27)$$

$$(M_{BC}^{\max})^{\max} = M_{BC}^{\max}\Big|_{\alpha=1-\beta_L} \quad (28)$$

4.3 Ideal nose specifications

Nose specifications should be optimized in a way that some main criteria can be achieved. At first, the values of station moment at the end of phases, $M_{B,1}\big|_{\alpha=1-\beta_L}$ and $M_{B,2}\big|_{\alpha=1}$, should approach to -1/12 as much as possible (the negative maximum value at service time). Moreover, the station moment during phase two of launching should not exceed the mentioned values. In this regard, with an adequate value for relative flexural stiffness to ensure $\beta_{EI} \geq 0.2$, the latter criterion can be controlled (See Fig. 4) [5]. In other words, taking $\beta_{EI} \geq 0.2$ provides the situation that the maximum and minimum moment of station take place at the ends points of phases. Therefore, the minimum condition of launching negative moment is obtained as follows:

$$M_{B,1}\Big|_{\alpha=1-\beta_L} = M_{B,2}\Big|_{\alpha=1} \quad (29)$$

Table 1 shows some proper values of relative nose length and relative nose weight results from the above relation using regression analysis. As can be seen, there is a positive correlation between these two nose specifications under negative moment conditions. It should be noted that nose stiffness and weight are related and therefore this relation should be considered in practical use.

Table 1. Appropriate values of β_q and β_L under minimum condition of negative moment.

β_L	0.593	0.634	0.667	0.706	0.730	0.760	0.792	0.840	0.940
β_q	0.05	0.08	0.1	0.12	0.13	0.14	0.15	0.16	0.169

Fig. 7a, b shows the envelope moments of stations B and C for different values of relative nose length and weight obtained from (29). As it is shown in Fig. 7a, b, for $\beta_q \geq 0.16$, the absolute maximum negative moment, takes place at the former station (station C). Therefore, limiting relative nose weight, as $0 \leq \beta_q \leq 0.16$, is the other thing that should be met.

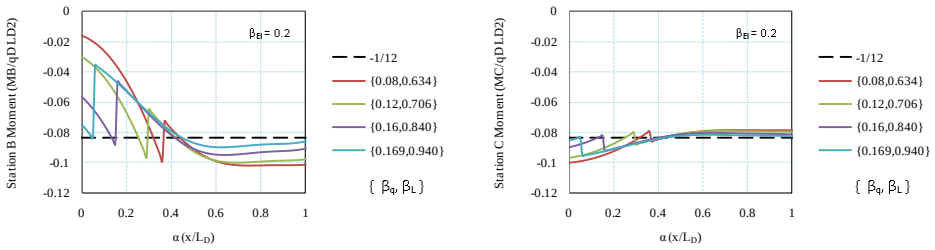

Figure 7. Envelope of moment under minimum condition of negative launching moment; a) Station B, b) Station C.

The last criterion is controlling the launching positive moments in spans AB and BC. Fig. 8a, b shows the envelope of maximum positive moment of these spans, by allocating the nose properties from equation (29). It can be concluded that as the relative nose weight and length are increased, the maximum positive moment is decreased during launching.

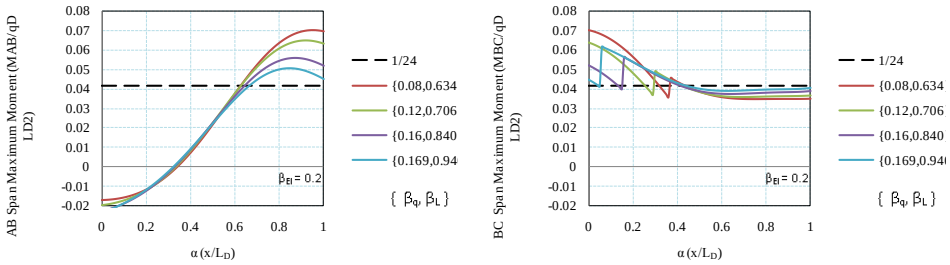

Figure 8. Maximum moment of spans under minimum condition of negative launching moment; a) Span AB, b) Span BC.

In order to minimize the absolute maximum positive moment under the minimum condition of negative moment, the value of the absolute maximum positive moment in span AB should be same with one in span BC as much as possible. As a result, the maximum positive moment is minimized considering the minimum condition of negative moment. To do so, equations (27) and (28) leads to the minimum condition of positive moments as follows:

$$M_{AB}^{\max}\Big|_{\alpha=1-\beta_q\beta_L} = M_{BC}^{\max}\Big|_{\alpha=1-\beta_L} \tag{30}$$

The relation between proper relative nose length and relative nose weight under the condition of minimum positive moment can be obtained through a regression analysis. Fig. 9 shows the proper relative nose length and relative nose weight under the both minimum negative and positive conditions.

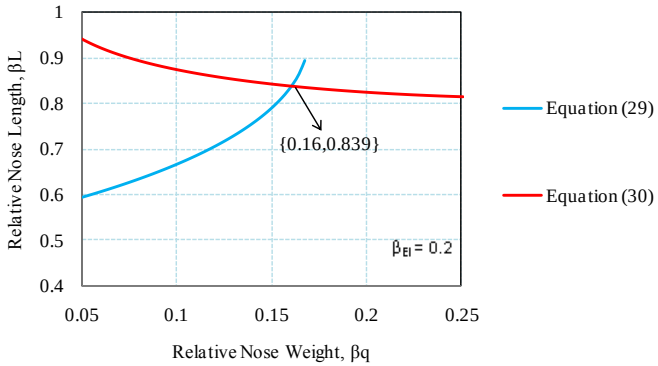

Figure 9. Relation between proper relative nose length and proper relative nose weight

In spite of the minimum negative condition, for the positive one, there is a negative correlation between relative nose length and weight. It is evident that the curves coincide with each other at $\beta_q = 0.16$ and $\beta_L = 0.839$. It is worthwhile to mention that these obtained values for nose specifications are

valid theoretically provided that $M_{AB}^{\max}$ occurs in deck section (not nose one). Nevertheless, for these values, $M_{AB}^{\max}$ occurs (when $\alpha = 0.866$) within a distance about 0.546 from support A. Therefore, the latter control is also met.

It can be concluded that, by choosing ideal specifications for nose, $\beta_q = 0.16$, $\beta_L = 0.839$ and $\beta_{EI} = 0.2$, all the above mentioned criteria will be satisfied (See Fig. 10a, b). It should be noted that nose specifications have strong relationships with construction costs. Besides, in practice, due to interdependency of nose characteristics, more complexities arise out of nose optimum design. In addition, by choosing a proper prestressing scheme may not be needed to satisfy all the foregoing criteria during launching. Therefore, some other engineering assessments should be taken into account. Nevertheless, this present study has paved the way for the future studies.

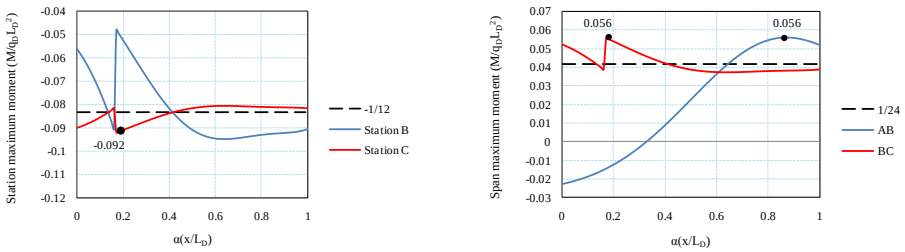

Figure 10. . Absolute maximum negative and positive moment for $\beta_q = 0.16$, $\beta_L = 0.839$ and $\beta_{EI} = 0.2$; a) Stations B & C, b) Spans AB & BC.

Remark II: The ideal values for nose parameters have been obtained based on a simple mathematical approach; however, for practical usages it is not feasible to satisfy all the aforementioned ideal criteria exactly. For this reason, majority of researchers have suggested economical and practical values as $\beta_q = 0.1$, $\beta_{EI} = 0.2$ and $\beta_L = 0.6 - 0.65$ (Rosignoli 1998); even if these values do not satisfy all the mentioned criteria. Fig. 11 shows the envelope of the fifteenth station moment for these values, considering $\beta_L = 0.65$. Moreover, to provide a validation for the current study, the results obtained by finite element method (FEM) is also presented in Fig. 11. For the FEM solution, 20 numbers of, two-node, two-dimensional beam elements are used per deck span. Proportionally, 13 numbers of elements are considered for the nose girder.

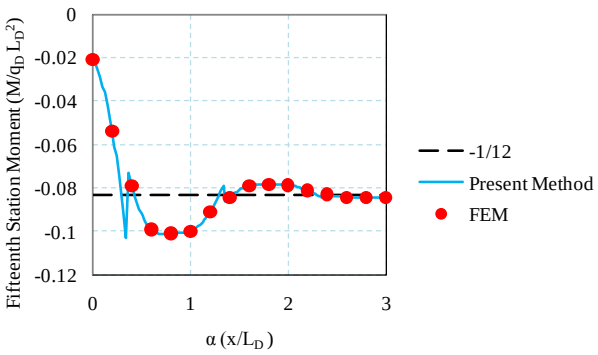

Figure 11. Envelope of the fifteenth station moment for $\beta_L = 0.65 \& 0.839$, $\beta_q = 0.1 \& 0.16$ and $\beta_{EI} = 0.2$.

4.4 Effects of temperature gradient and shear strain

Hereinafter, practical values discussed in Remark II are considered for nose specifications to study the influence of other parameters on nose-deck interaction. Fig. 12 shows the effects of different temperature gradients on the performance of nose-deck system during launching. β_{HN} and β_{HD} are assumed to be 1/20 and 1/10, and the coefficients of thermal expansion for concrete and steel materials are assumed to be 11.3×10^{-6} 1/C° and 8.5×10^{-6} 1/C°, respectively. Negative gradient (higher temperature in the upper part of the section) makes the condition worse but the change of the envelope of the station moment due to this phenomenon is not significant in general (Fig. 12)

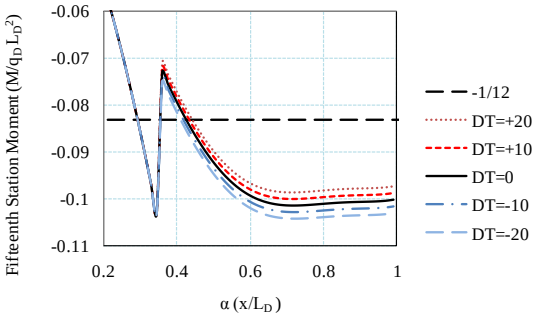

Figure 12. Envelope of the fifteenth station moment with different temperature gradients.

Fig. 13 shows the envelope of the station moment with respect to the shear strain effect on the beam. This effect is considered by setting $\beta_s = 3.2$ and

different values of β_r. $\beta_s = 0$ corresponds to the situation when shear strain is neglected. Generally, for composite box girders, β_r is less than 0.02 [20]. Therefore, shear strain effect can be negligible in most practical cases.

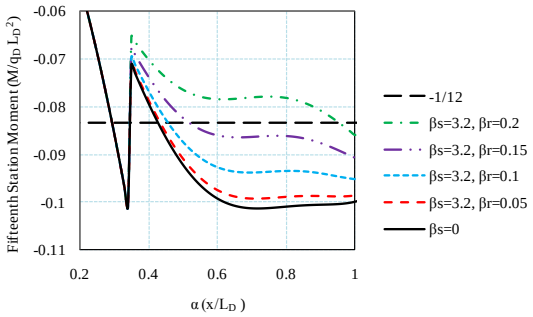

Figure 13. Envelope of the fifteenth station moment regarding the shear strain effect.

5 DISCUSSION ON THE SIMPLIFIED CONVENTIONAL MODEL

As mentioned in Section. Nose-Deck Interaction, structural behavior of the launching bridge tends to a continuous beam when there are infinite number of spans behind the under study station. Marchetti (1984) proposed the rotation of the section B (θ_B), as in Fig. 6a, b, as follows:

$$\theta_B = a_1 M_B + a_2, \quad a_1 = \frac{1}{2\sqrt{3}E_D I_D} \approx 0.288675 \frac{1}{E_D I_D}, \quad a_2 = \frac{q_D L_D{}^3}{24\sqrt{3}E_D I_D} \approx 0.024056 \frac{q_D L_D{}^3}{E_D I_D} \tag{31}$$

where, a_1 and a_2 are constant coefficients dependant on deck specifications only. By using this relation for any station of deck, the problem can be reduced to analyze a continuous beam with lower degrees of indeterminacy. It is intuitively obvious that the values proposed in (31) are not valid for initial stages of launching. Therefore, in the current study the precision of conventional beam model for initial stages, via matrix structural analysis, is evaluated. In other words, it begs this question that in what extend considering infinite number of spans behind the station under study is accurate.

Fig. 14a, b, c, d illustrates envelop of rotation for stations 2 to 5. In this figure it is assumed that all spans are identical and β_0 is zero. Also the behavior of fifteenth station is shown in this figure to represent a station with infinite number of spans behind it. The superscript (*) implies that the rotation is

obtained by (31). A glimpse into the obtained results reveals that stations two to five (except station three) are more critical than farther ones during their relevant stages. It can be concluded that exact behavior of these stations, especially stations two and four, are different from the results obtained by conventional semi-infinite beam model. However, results for station five to the next ones completely match to the Marchetti's formulation. As a result, due to conventional semi-infinite beam assumptions, the bridge does not reach to its infinite continuous scheme at initial stages of launching. Therefore, it can be concluded that (31) is only valid when there are at least 5 spans behind the studied station. It is worth noting, similar drawback can be seen for the moment of stations as in Fig. 15. In a nutshell, as using the conventional beam model is inevitable for optimization of nose-deck interaction, it entails a simple modification to be applied for initial stages or bridges with fewer numbers of spans. This modification pertains to find a_1 and a_2 coefficients based on the relation between moment and rotation for initial stations.

Numerical studies have been made for station two in second stages and also for station three in third stage of launching. Table. 2 presents the modified values for a_1 and a_2 for different values of β_1 and β_0.

Table 2. Modified values of a_1 and a_2 for different values of β_1 and β_0

β_1		1			0.9			**0.85**			0.8		
β_0		0	0.5	0.75	0	0.5	0.75	0	**0.5**	0.75	0	0.5	0.75
St.2	a_1	0.3325	0.3337	0.3334	0.3	0.3	0.3	0.2834	**0.2833**	0.2834	0.2667	0.2666	0.2667
	a_2	0.0416	0.0396	0.037	0.0304	0.0285	0.0262	0.0256	**0.0238**	0.0216	0.0213	0.0197	0.0176
St.3	a_1	0.2916	0.2917	0.2917	0.2895	0.2895	0.2895	0.2883	**0.2883**	0.2883	0.287	0.287	0.287
	a_2	0.0208	0.0214	0.022	0.0227	0.0232	0.0238	0.0235	**0.024**	0.0246	0.0242	0.0246	0.0252

The provided coefficients can be replaced in (31) to modify the relation for initial stations. Since, a_1 and a_2 are nearly equal to values given by (31), bolded values for β_1 and β_0 ($\beta_1 = 0.85$ and $\beta_0 = 0.5$) are suitable to make initial stations behavior close to farther ones. It should be noted that a_1 and a_2 are completely independent of geometrical and mechanical specifications of nose.

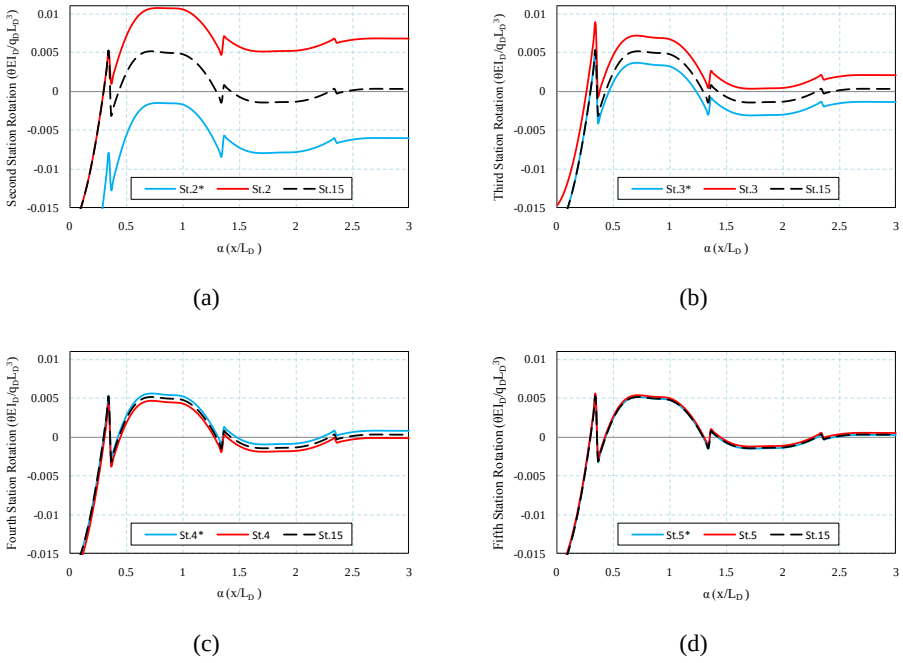

Figure 14. Envelope of rotation for some initial stations; a) Station 2, b) Station 3, c) Station 4, d) Station 5.

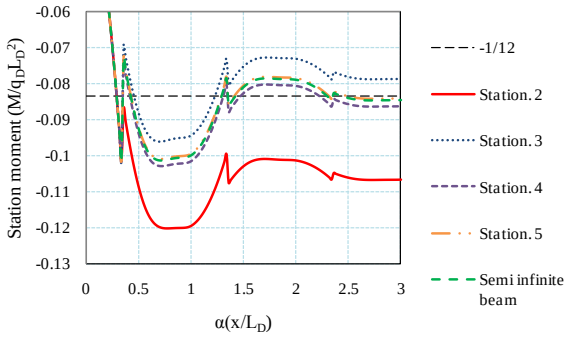

Figure 15. Envelope of the moment for initial stations during their launching stages.

6 RESOLVING THE NOSE-DECK INTERACTION FOR INITIAL STAGES

In the majority of investigations deal with proper optimization of nose parameters, as in [5] and [10], the proper practical values are obtained based on semi-infinite beam model. However, to preserve the optimum nose parameters for all stages, and also bridge with fewer number of spans (i.e. less than five piers), two main solutions can be suggested:

1. Keeping some parts of deck segments on the construction platform. In fact, in the practical projects, a piece of superstructure is usually kept on the platform in each stage of launching over the half length of the mid span.
2. Increasing bending stiffness of second station by shortening length of the first span.

In construction process and service time, first span undergoes the maximum absolute negative and positive moment. Consequently, not only does the latter solution reduce temporary construction tensions significantly but also optimizes static performance of the bridge during service time.

As an example, Fig. 16a, b shows the scenario of internal bending moment of superstructure parts during launching phases one and two of stage eighth. Temperature effects, support settlements, shear deformation and platform loads are neglected and all spans are considered to be identical. As this figure shows bridge spans, except some initial and end ones, perform like clamped beams. Therefore; moments at these supports and midpoints are approximately as –1/12 and +1/24, respectively.

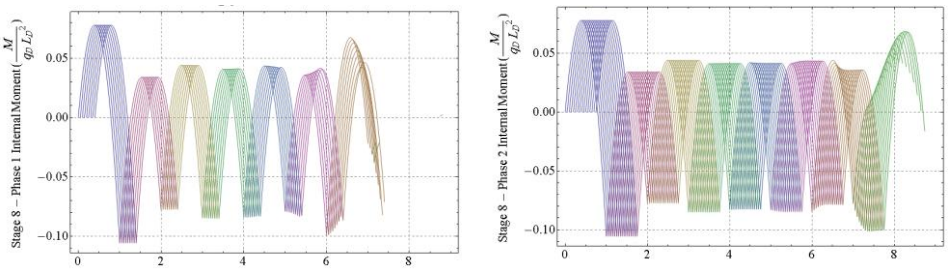

Figure 16. Scenario of internal bending moment of eighth stage; a) phase 1, b) phase 2.

Fig. 17 illustrates envelope of moment for station 2 in second stage of launching, considering optimum values of β_1 and β_0 versus that of obtained by considering β_1 and β_0 as 1 and 0, respectively. This figure indicates that by choosing the optimum values, envelop of moment for station 2 in second stage

of launching thoroughly conforms to envelop of moment for station 15 in fifteenth stage of launching.

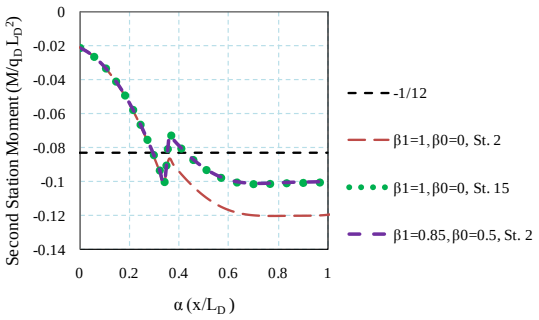

Figure 17. Envelope of moment for station 2 in second stage of launching with optimum values of β_1 and β_0.

Fig. 18a, b shows internal moment diagram of deck in an instant of launching eighth stage (when nose tip distance from the first pier is 9.5 (in normalized format) for β_1 equal to 1 and 0.85. It can be concluded that not only does choosing optimum values for β_1 and β_0 optimize the launching moment of initial stations in their launching stages but also such a treatment resolves and closes moment of different stations during all stages of launching.

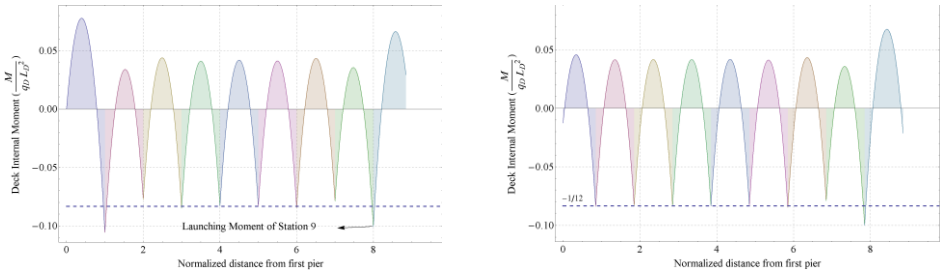

Figure 18. Moment diagram of deck in eighth stage; a) $\beta_1 = 1$, b) $\beta_1 = 0.85$.

All in all, similar moment diagram can be obtained while launching the bridge is finished, and the construction platform will be removed ($\beta_0 = 0$), which is similar to the moment diagram at service life by considering dead loads. Therefore, it can be concluded that the suggested value for β_1 can optimize the static performance of bridge in service time, as well.

7 CONCLUSIONS

A new model based on matrix structural analysis has been developed for incremental bridge launching. The model is capable of simulating the static behavior of bridge during different construction stages. Also some factors such as support settlement, shear strain, temperature gradient, and construction platform are regarded in the model for analysis. In addition, using a simple approach has led the analysis to scale all parameters involved in the problem with respect to main specifications of deck. As a result, it is much worthy to have parametric study of the problem. An investigation has been made into the envelope of the moment and rotation of stations during launching. In turn, two boundary conditions obtained for the previous stations. In this way, a simplified model (semi-infinite beam) is risen up with less degree of freedom which is very useful for parametric study on nose-deck interaction system. This conventional model is considered as a prototype model to be used for optimization of nose-deck interaction. Likewise, a new simple mathematical approach is introduced for optimization of nose performance during launching. This approach pertains to find some optimum ranges for nose lengths, nose weight and nose flexural stiffness with respect to some criteria. However, in the primary studies of authors, such a treatment does not take the interdependency of optimization parameters into account, and only the ideal specifications of nose is presented based on its optimum structural performance. However, proper optimization of nose girder entails some others engineering and economic assessments to be incorporated in the proper design of nose. At this aim, the present study may pave the road for future investigations into ideal design of nose. In addition, an extensive study has been done to assess the accuracy of semi-infinite beam model. It has been concluded that this model is only accurate when there are at least five spans behind the under study station which means that the model is not useful for studying initial stages of launching and bridges with few numbers of spans. In this regard, the effects of first span length and construction platform have been taken into account and the formulations for semi-infinite beam model are modified based on these effects. To keep the advantageous of the optimal designed nose for all stages of launching, as well as initial ones, the optimum values of first span and platform length have been obtained. It has been demonstrated, these optimum values make the behavior of initial stations identical to farther ones and ameliorates the static performance of bridges in service time after launching is passed.

REFERENCES

[1] The Concrete Society, Incremental launching - Applications. [Online] 2013. http://concrete.org.uk/fingertips_nuggets.asp?cmd=display&id=383.

[2] Rosignoli, M, *Bridge launching*, Thomas Telford, London, 2002.

[3] Marzouk, M, El-Dein, H Z, and El-Said, M, "Application of computer simulation to construction of incremental launching bridges." Journal of Civil Engineering and Management, Vol. 13, No. 1, pp. 27-36, 2007.

[4] Zellner, W, and Svensson, H, "Incremental launching of structures" Journal of Structural Engineering, Vol. 109, No. 2, pp. 520–37, 1983.

[5] Rosignoli, M, "Nose-deck interaction in launched prestressed concrete bridges", Journal of Bridge Engineering, Vol. 3, No. 1, pp. 21–27, 1998.

[6] AASHTO, *Bridge construction practices using incremental launching*, Highway Subcommittee on Bridges and Structures, 2007.

[7] Rosignoli, M, "Prestressing Schemes for Incrementally Launched Bridges", Journal of Bridge Engineering, Vol. 4, No. 2, pp. 107-115, 1999.

[8] Sasmal, S, and Ramanjaneluyu, K, "Transfer matrix method for construction phase analysis of incrementally launched prestressed concrete bridges", Journal of Engineering Structures, Vol. 28, No. 13, pp. 1897-1910, 2006.

[9] Marchetti M. E, "Specific design problems to bridges built using the incremental launching method", Journal of Engineering Structures, Vol. 6, No. 3, pp. 185–210, 1984.

[10] Fontan, AN, Diaz, J, M, Baldomir, A, and Hernandez, S, "Improved Optimization Formulations for Launching Nose of Incrementally Launched Prestressed Concrete Bridges", Journal of Bridge Engineering, Vol. 16, No. 3, pp. 461–470, 2011.

[11] Rosignoli, M, "Reduces-Transfer-Matrix Method for Analysis of Launched Bridges", ACI Structural Journal, Vol. 96, No. 4, 603–608, 1999.

[12] Sasmal, S, Ramanjaneluyu, K, Srinivas, V., and Gopalakrishnan, S, "Simplified Computational Methodology for Analysis and Studies on Behavior of Incrementally Launched Continuous Bridges", Journal of Structural Engineering and Mechanics, Vol. 17, No. 2, pp. 245-266, 2004.

[13] Arici, M, and Granata, MF, "Analysis of curved incrementally launched box concrete bridges using the transfer matrix method", Journal of Bridge Structures, Vol. 3, No. 3-4, pp. 165–181, 2007.

[14] Granta, M, Margiotta, P, Arici, M, "A Parametric Study of Curved Incrementally Launched Bridges." Journal of Engineering Structures, Vol.49, pp. 373–384, 2013.

[15] Lee, HW., Ahn, TW., Kim, KY, "Nose-Deck Interaction in ILM Bridge Proceeding with Tapered Sectional Launching Nose." *Computational Mechanics, Beijing, China,* 2004.

[16] Jung, K, Kim, K, Sim, CW., and Jay Kim, JH, "Verification of Incremental Launching Construction Safety for the Ilsun Bridge, the World's Longest and Widest Prestressed Concrete Box Girder with Corrugated Steel Web Section." Journal of Bridge Engineering, Vol. 16, No.3, pp. 453-460, 2011.

[17] Nie, JG, and Cai, CS, "Steel–Concrete Composite Beams Considering Shear Slip Effects", Journal of Structural Engineering, Vol. 129, No. 4, pp. 495-506, 2003.

[18] Nie, JG, Cai, CS., Zhou, TR, and Li, Y, "Experimental and Analytical Study of Prestressed Steel–Concrete Composite Beams Considering Slip Effect", Journal of Structural Engineering, Vol. 133, No. 4, pp. 530-540, 2007.

[19] Sennett, R, "*Matrix Analysis of Structures*", Waveland Press, 2000.

[20] Sennah, K, Kennedy, JB, and Nour, S, "Design for Shear in Curved Composite Multiple Steel Box Girder Bridges." Journal of Bridge Engineering, Vol. 8, No. 3, pp. 144–152, 2003.

Received: Feb. 21, 2014 Accepted: May 7, 2014